

This discussion paper is/has been under review for the journal Atmospheric Chemistry and Physics (ACP). Please refer to the corresponding final paper in ACP if available.

**Hygroscopic
properties of
Amazonian biomass
burning**

E. O. Fors et al.

Hygroscopic properties of Amazonian biomass burning and European background HULIS and investigation of their effects on surface tension with two models linking H-TDMA to CCNC data

E. O. Fors¹, J. Rissler¹, A. Massling^{1,****}, B. Svenningsson¹, M. O. Andreae², U. Dusek^{2,*}, G. P. Frank^{2,**}, A. Hoffer^{2,***}, M. Bilde³, G. Kiss⁴, S. Janitsek⁴, S. Henning⁵, M. C. Facchini⁶, S. Decesari⁶, and E. Swietlicki¹

¹Lund University, Department of Physics, Division of Nuclear Physics, Lund University, Lund, Sweden

²Max Planck Institute for Chemistry, Department of Biogeochemistry, Mainz, Germany

³University of Copenhagen, Department of Chemistry, Copenhagen, Denmark

Title Page

Abstract

Introduction

Conclusions

References

Tables

Figures

⏪

⏩

◀

▶

Back

Close

Full Screen / Esc

Printer-friendly Version

Interactive Discussion

**Hygroscopic
properties of
Amazonian biomass
burning**E. O. Fors et al.

[Title Page](#)[Abstract](#)[Introduction](#)[Conclusions](#)[References](#)[Tables](#)[Figures](#)[⏪](#)[⏩](#)[◀](#)[▶](#)[Back](#)[Close](#)[Full Screen / Esc](#)[Printer-friendly Version](#)[Interactive Discussion](#)

⁴ University of Veszprém, Air Chemistry Group of the Hung. Acad. of Sciences,
Veszprém, Hungary

⁵ Leibniz-Institute for Tropospheric Research, Department of Physics, Leipzig, Germany

⁶ Istituto di Scienze dell'Atmosfera e del Clima – CNR, Bologna, Italy

* now at: Institute for Marine and Atmospheric Research, Utrecht University,
Utrecht, The Netherlands

** now at: Lund University, Department of Physics, Division of Nuclear Physics, Lund University,
Lund, Sweden

*** now at: University of Veszprém, Air Chemistry Group of the Hung. Acad. of Sciences,
Veszprém, Hungary

**** now at: National Environmental Research Institute, Department of Atmospheric
Environment, Aarhus University, Roskilde, Denmark

Received: 6 December 2009 – Accepted: 7 December 2009 – Published: 15 December 2009

Correspondence to: E. O. Fors (erik.fors@nuclear.lu.se)

Published by Copernicus Publications on behalf of the European Geosciences Union.

Abstract

HUmic-Like Substances (HULIS) have been identified as major contributors to the organic carbon in atmospheric aerosol. The term HULIS is used to describe the organic material found in aerosol particles which resembles the humic organic material in river and sea water and in soils. In this study two sets of filter samples from atmospheric aerosols were collected at different sites. One sample was collected at the K-pusztá rural site in Hungary, about 80 km SE of Budapest, and a second set of samples was collected at a site in Rondônia, Amazonia, Brazil, during the LBA-SMOCC biomass burning season experiment. HULIS were extracted from the samples, and their hygroscopic properties were studied using a Hygroscopicity Tandem Differential Mobility Analyzer (H-TDMA) at relative humidity (RH) <100%, and a cloud condensation nucleus counter (CCNC) at RH >100%. The H-TDMA measurements were carried out at a dry diameter of 100 nm and for RH ranging from 30 to 98%. At 90% RH the HULIS samples showed diameter growth factors between 1.04 and 1.07, reaching values of 1.4 at 98% RH. The cloud nucleating properties of the two sets of aerosol samples were analyzed using two types of thermal static cloud condensation nucleus counters (CCNC). Two different parameterization models were used to investigate the potential effect of HULIS surface activity, both yielding similar results. For the K-pusztá winter HULIS sample, the surface tension at the point of activation was estimated to be lowered by between 34% (47.7 mN/m) and 31% (50.3 mN/m) for dry sizes between 50 and 120 nm in comparison to pure water. A moderate lowering was also observed for the entire water soluble aerosol sample, including both organic and inorganic compounds, where the surface tension was decreased by between 2% (71.2 mN/m) and 13% (63.3 mN/m).

ACPD

9, 26925–26967, 2009

Hygroscopic properties of Amazonian biomass burning

E. O. Fors et al.

Title Page

Abstract

Introduction

Conclusions

References

Tables

Figures

⏪

⏩

◀

▶

Back

Close

Full Screen / Esc

Printer-friendly Version

Interactive Discussion

1 Introduction

Aerosol particles play an important role in the atmosphere via their influence on the radiative budget of the earth by directly scattering and absorbing the incoming sunlight (e.g., Ramanathan et al., 2001; Satheesh and Moorthy, 2004), and indirectly by serving as cloud condensation nuclei (CCN) for the formation of cloud droplets (e.g., Kaufmann et al., 2002; Andreae and Rosenfeld, 2008). The indirect effect is dependent on particle hygroscopicity at water vapour supersaturated conditions, more specifically the saturation ratio needed to activate the CCN into forming a cloud droplet. The properties of the CCN are important to understand the cloud formation processes and to predict the resulting droplet size distributions determining the cloud albedo and cloud lifetime (e.g., Warner, 1967; Rosenfeld, 2000), parameters that are strongly linked to the indirect aerosol effect.

The atmospheric aerosol is known to contain a complex mixture of different chemical compounds comprising inorganic as well as organic constituents. The fraction of organic material in the atmospheric aerosol varies strongly, and reports on the fine fraction (particle diameter, $D_p < 1 \mu\text{m}$) state values varying between 20 and 80% in the US alone (Jacobson et al., 2000). Out of this organic fraction, about 10–60% has been found to be Water Soluble Organic Carbon (WSOC) (Krivacsy et al., 2001; Kleefeld et al., 2002; Young et al., 2004). Up to now, the knowledge about the hygroscopic growth and CCN properties of the multitude of water-soluble organic compounds found in aerosol particles is very limited (Kanakidou et al., 2005).

Even though the super micron particles constitute most of the particle mass, the dominant number of particles in atmospheric samples is found in the submicron size range and thus their hygroscopic properties are of high importance. It has been shown that some of the water soluble organic compounds (WSOC) are surface active and might affect the water uptake and cloud droplet activation of aerosol particles, not only by contributing to the soluble mass but also by reducing the surface tension (Graber et al., 2006; Facchini et al., 2000; Charlson et al., 2001; Nenes et al., 2002). It has

Hygroscopic properties of Amazonian biomass burning

E. O. Fors et al.

Title Page

Abstract

Introduction

Conclusions

References

Tables

Figures



Back

Close

Full Screen / Esc

Printer-friendly Version

Interactive Discussion

Hygroscopic properties of Amazonian biomass burning

E. O. Fors et al.

Title Page

Abstract

Introduction

Conclusions

References

Tables

Figures

⏪

⏩

◀

▶

Back

Close

Full Screen / Esc

Printer-friendly Version

Interactive Discussion

also been discussed whether or not surface to bulk partitioning is an important effect in atmospheric aerosols. It has been shown that surface partitioning of some components, such as fatty acids, can affect the critical supersaturation, resulting in an increased molecule concentration at the surface of the particle at the expense of the bulk concentration of that particular component (Sorjamaa et al., 2008; Prisle et al., 2007; Prisle et al., 2009). As the particle takes up water, the volume to surface ratio increases, which leads to a migration of molecules from the surface to the bulk.

A typical aerosol sample can be described in terms of the inorganic and the total carbonaceous fraction. The total carbonaceous matter can be subdivided into the water insoluble organic matter plus black carbon and the water soluble organic matter. The water soluble organic matter can be further subdivided into more hydrophilic organic matter and a less hydrophilic organic fraction called isolated organic matter (ISOM), which is mostly HUmic-Like Substances (HULIS), characterized by relatively long chains of organic molecules (Fig. 1). These can originate from a number of sources. Biomass burning (Mayol-Bracero et al., 2002), polymerization in the aerosol aqueous phase (Gelencser et al., 2002), oxidation of soot (Decesari et al., 2002) and acid catalyzed reaction of isoprenoids and terpenoids (Limbeck et al., 2003) are examples of possible origins. HULIS are significant contributors to the organic fraction of the atmospheric aerosol in various environmental reservoirs and an evaluation of hygroscopic and CCN nucleating properties of HULIS is an important task to further understand the role of organic carbon in cloud formation processes and to quantitatively evaluate the contribution from HULIS in this context.

Several experimental studies have been conducted on the hygroscopic properties of HULIS, giving quite diverse results, due to the vast number of species that can fall under the HULIS definition, since HULIS is ultimately defined by the separation method used in the isolation procedure of the sample. Gysel et al. (2004), Dinar et al. (2006) and Ziese et al. (2007) all determined the hygroscopic properties of isolated HULIS samples, measuring hygroscopic growth factors between 1.05 and 1.24 at 90% RH.

In this study, the hygroscopic and CCN nucleating properties of two sets of atmospheric samples were investigated using a Hygroscopic Tandem Differential Mobility Analyser (H-TDMA) and two different cloud condensation nuclei counters (CCNC). Connecting these data sets, two different parameterization models were used to quantify the possible surface tension altering effects of the HULIS fraction. One model extrapolates H-TDMA data to supersaturation to predict the critical supersaturation ratio, while the other model uses an iterative scheme, requiring both H-TDMA and CCNC data, to obtain a concentration dependent parameterization of the surface tension.

2 Samples

A set of six samples was taken during the LBA-SMOCC campaign in Rondônia, Brazil, 17 September–4 October 2002, during the dry period. Rondônia is a region with high rates of deforestation and biomass burning. The sampling time varied between 36 and 84 h. Three samples were taken during daytime hours only, while three other samples were taken during the night time, named “SMOCC D1”, “SMOCC D2”, “SMOCC D3”, “SMOCC N1”, etc., where D and N denote Day and Night sample, and the numbers represent the collection periods. The three intervals are 17–21 September (period 1), 21–28 September (period 2) and 28 September to 4 October (period 3). The samples were collected with a high volume sampler, with a cut-off diameter of 2.5 μm , meaning that all particles with an aerodynamic diameter less than 2.5 μm were deposited on a filter. A detailed description of the aerosol sampling and chemical measurements performed during the SMOCC experiment can be found in Decesari et al. (2006) and in Fuzzi et al. (2007). The limited collected mass of each sample made only one type of measurement per sample possible, either using the H-TDMA or the CCNC. Table 1 shows which samples were used for which measurements. For the SMOCC samples, only isolated HULIS samples were available.

A set of two 24-h samples was taken at the K-pusztá rural site ca. 80 km south of Budapest, Hungary, during 16 February and 11 July 2001. The sampling station was

Hygroscopic properties of Amazonian biomass burning

E. O. Fors et al.

Title Page

Abstract

Introduction

Conclusions

References

Tables

Figures



Back

Close

Full Screen / Esc

Printer-friendly Version

Interactive Discussion



situated on a forest clearing on the Great Hungarian Plain. A more detailed description of the site can be found in e.g. Pio et al. (2007). These samples are denoted K-pusztá *winter* and *summer*. The samples were collected on quartz fibre filters with a high volume sampler, with a cut-off of 1.5 μm . Unlike the SMOCC samples, each K-pusztá sample resulted in three types of sub-samples: extract, effluent and HULIS (defined in the following section). Each sample was evaluated both using the H-TDMA and the CCNC for all samples except for the summer HULIS sample. Table 1 lists the determined set of aerosol samples.

3 Extraction

First, the water-soluble aerosol components were extracted by placing the filters for 24 h in MilliQ water. Then the extract was filtered through a Millipore membrane filter of 0.45 μm pore size (the remaining sample from here denoted as *extract*) and the pH was adjusted to pH=2 with hydrochloric acid. The separation of HULIS from other dissolved components was performed on Oasis HLB (Waters, USA) solid phase extraction (SPE) columns. Typically 60% of the water-soluble organic carbon content is retained under these conditions, while inorganic ions passed through the SPE columns together with the most hydrophilic organic compounds (*effluent*). The retained organic compounds, in the method denoted ISOM, were eluted with methanol. The methanol eluate was evaporated to dryness, and known portions of the isolated organic matter were re-dissolved in water prior to H-TDMA and CCNC measurements. A detailed discussion of the SPE procedure, including column selection and performance, can be found in Varga et al. (2001). In this work the ISOM fraction is hereafter referred to as HULIS, in consistency with literature. This procedure was conducted on all samples. For the K-Pusztá samples, all fractions were saved and analysed. However, for the SMOCC samples, only the HULIS was saved for analysis, as there were at this point no plans of analysing the extract and effluent samples.

Hygroscopic properties of Amazonian biomass burning

E. O. Fors et al.

Title Page

Abstract

Introduction

Conclusions

References

Tables

Figures

⏪

⏩

◀

▶

Back

Close

Full Screen / Esc

Printer-friendly Version

Interactive Discussion

4 Methods

For both the H-TDMA and the CCNC measurements, monodisperse aerosol particles were generated from the solutions using a small nebulizer, dried in diffusion dryers, diluted with clean oil-free air and then given a well defined charge distribution with a bipolar charger.

4.1 H-TDMA measurements

The measurements of hygroscopic growth at subsaturation were carried out using an H-TDMA system (Hygroscopicity Tandem Differential Mobility Analyzer) (Swietlicki et al., 2007) with the same instrumental setup used by, e.g., Svenningsson et al. (2006). The H-TDMA consists of two DMAs with a humidifier as conditioning section in between. The first DMA selects a monodisperse fraction of the aerosol while the second DMA in combination with a condensation particle counter (CPC) analyzes the altered size distribution after humidification to a specific RH. Both DMAs were operated as open end systems, with humidity controlled for both the aerosol and for the sheath air flow. This was done through water-to-gas Gore-Tex® membranes, with regulation of the temperature of the surrounding water and mixing of dry and humidified air for the control of the aerosol and sheath air flows, respectively, and with mass flow controllers mixing humid and dry air. This setup enables measurements of both possible deliquescence and efflorescence behaviour of the aerosol. Measurements were made for particles with an initial electrical mobility equivalent dry DMA1 diameter of 100 nm at DMA2 relative humidity (RH) values between 30% and 98%. Measurements at high RH were controlled by test salt measurements of known hygroscopic growth to determine the exact RH during the growth measurements. The result is presented as measured hygroscopic growth factor, Gf , defined according to

$$Gf = \frac{D_{\text{drop}}}{D_p} \quad (1)$$

Hygroscopic properties of Amazonian biomass burning

E. O. Fors et al.

Title Page

Abstract

Introduction

Conclusions

References

Tables

Figures

⏪

⏩

◀

▶

Back

Close

Full Screen / Esc

Printer-friendly Version

Interactive Discussion



where D_{drop} is the droplet diameter and D_p is the dry diameter of the particle.

4.2 CCN counter measurements

To determine the size-dependent activation curve of the investigated aerosol, a narrow size fraction was selected using a DMA (TSI, Model 3080). The monodisperse aerosol was divided between a condensation particle counter (TSI, Model 3010) and a static thermal-gradient CCN chamber.

The size dependent CCN properties of the SMOCC particles were determined with a static thermal-gradient CCN counter from the Max Planck Institute for Chemistry (MPIC), Mainz. The main part of the CCN counter is an 80 mm diameter chamber with a distance of 10 mm between the upper and lower plate. The plates are continuously kept wetted and their temperature difference is controlled to define the supersaturation in the chamber. Various supersaturation ratios, s_c , can be adjusted. The device uses laser illumination and a video camera for detection of activated droplets. The two CCN counters were intercalibrated, using the calibration procedure described in Frank et al. (2007). The activation of particles of dry diameters between 40 and 125 nm was studied. At each measurement the particle diameter was kept fixed and the supersaturation was changed stepwise. For the SMOCC samples, the error estimates for the critical supersaturation are 95% confidence intervals. The uncertainty was calculated using two methods. Firstly, a cumulative Gaussian (normal) distribution function which was fitted to each CCN spectrum to derive a midpoint activation diameter (d_a) of the aerosol, defined as the diameter at which the cumulative Gaussian function reaches half its maximum height. In addition, the uncertainty if the supersaturation setting of the instrument was calculated according to Frank et al. (2007). It turned out that the supersaturation setting of the instrument is the major part of the uncertainty.

The size dependent CCN properties of the K-pusztá particles were determined using a static thermal-gradient diffusion CCN chamber from the University of Wyoming, model CCNC-100B. This CCN counter uses the same principle for generating the supersaturation as the Mainz CCN counter described above, while the centre axis of the

Hygroscopic properties of Amazonian biomass burning

E. O. Fors et al.

Title Page

Abstract

Introduction

Conclusions

References

Tables

Figures

⏪

⏩

◀

▶

Back

Close

Full Screen / Esc

Printer-friendly Version

Interactive Discussion



**Hygroscopic properties of
Amazonian biomass
burning**E. O. Fors et al.

[Title Page](#)[Abstract](#)[Introduction](#)[Conclusions](#)[References](#)[Tables](#)[Figures](#)[⏪](#)[⏩](#)[◀](#)[▶](#)[Back](#)[Close](#)[Full Screen / Esc](#)[Printer-friendly Version](#)[Interactive Discussion](#)

chamber is illuminated by a laser diode (670 nm) and the activated droplets are detected by measuring the forward scattered light intensity at an angle of 45 degrees to the diode light beam. The CCNC-100B was calibrated using monodisperse sodium chloride and ammonium sulphate particles as in Bilde and Svenningsson (2004). For the K-pusztas samples, the error estimates for the critical supersaturation are 95% confidence intervals based on the calibration data for the CCN spectrometer. Sodium chloride and ammonium sulphate were used for the calibration. A van't Hoff factor of 2 was used for sodium chloride whereas for ammonium sulfate, it was adopted from the literature (Low, 1969; Young and Warren, 1992) and ranges between 2.2–2.4 at the point of activation. H-TDMA data on sodium chloride supports the use of a shape factor for a cube, i.e. 1.08. This shape factor also resulted in a better agreement between the ammonium sulphate and sodium chloride data compared to a unity shape factor and was thus used for the sodium chloride data in this case.

4.3 CCN modelling

There are a number of different model parameterizations available for calculating critical supersaturation ratios by extrapolating H-TDMA data into the supersaturated regime. All model parameterizations rely on an assumption of the value of the surface tension as a function of surfactant concentration. In this work we use two single parameter models: κ_R introduced by Rissler et al. (2004), also described in Vestin et al. (2006), and ρ_{ion} from Ziese et al. (2007). Both of them are based on the Köhler equation:

$$\rho_w = (D_p) = \rho^0 a_w \exp\left(\frac{4M_w \sigma}{RT \rho_w D_{drop}}\right) \quad (2)$$

where ρ_w is the water vapour pressure, ρ^0 the saturation water vapour pressure, a_w the activity of water in solution, M_w the molar weight of water, σ the surface tension,

R the universal gas constant, T the temperature, ρ_w the density of water, and D_{drop} the droplet size.

In addition to the two models used in this work, Petters and Kreidenweis (2007) have suggested an approach based on a single parameter, also named κ , defined through its effect on the water activity of the solution. Kreidenweis et al. (2005) suggested a similar definition, but with a polynomial expression included, to take non-ideal effects into account. That approach has the drawback of requiring growth factors at three or more RH values, in contrast to the other models requiring growth factors at only one RH. All the mentioned models have equally correct ways of describing the hygroscopicity of a particle. In this work we prefer to use the parameters κ_R and ρ_{ion} due to their intuitive physical meaning, namely the number of soluble entities per dry volume unit.

4.3.1 κ_R model

In the first model the number of soluble entities per volume unit is calculated from the measured hygroscopic growth factor, Gf , according to (Köhler theory assuming volume additivity)

$$Gf = \sqrt[3]{1 + \kappa_R \cdot \chi_\phi \cdot \frac{M_w}{\rho_w} \cdot \frac{a_w}{1 - a_w}} \quad (3a)$$

or rearranged

$$\kappa_R = \frac{(Gf^3 - 1) \cdot (1 - a_w)}{a_w \cdot \chi_\phi \cdot \frac{M_w}{\rho_w}} \quad (3b)$$

where κ_R is the number of soluble entities per volume dry unit, M_w the molecular weight of water, ρ_w the water density, and χ_ϕ a correction term introduced to account for non-ideal behaviour. The correction term is here determined using a model salt, assuming that the non-ideality of the solution can be described by the non-ideality of the model

Title Page

Abstract

Introduction

Conclusions

References

Tables

Figures

⏪

⏩

◀

▶

Back

Close

Full Screen / Esc

Printer-friendly Version

Interactive Discussion



Hygroscopic properties of Amazonian biomass burning

E. O. Fors et al.

Title Page

Abstract

Introduction

Conclusions

References

Tables

Figures

⏪

⏩

◀

▶

Back

Close

Full Screen / Esc

Printer-friendly Version

Interactive Discussion



salt at the same a_w . The model is also tested assuming ideal behaviour ($\chi_\phi=1$). This is in principle the same equation as later used in Petters and Kreidenweis (2007), but with a somewhat different definition of the parameter, κ . Following the approach of previous publications where the κ_R model has been applied (Rissler et al., 2004; Vestin et al., 2006; Rissler et al., 2006) ammonium sulphate was used as the model salt, since this is common and often the dominating inorganic compound in many atmospheric aerosols. The water activity correction term (χ_ϕ) is derived from Putokuchi et al. (1995), Tang et al. (1994) and at higher water activities from Low (1969).

The critical water vapour supersaturation, s_c , (S_c-1) can be approximated by the following equation is determined by the approximated expression of the Köhler theory, similar to that derived in Seinfeld and Pandis (2006):

$$s_c = \sqrt{\frac{4A^3}{27C} \cdot \frac{1}{\kappa_R \cdot \chi_\phi \cdot D_p^3}} \quad (4)$$

where A and C are defined as

$$A = \frac{4M_w\sigma}{RT\rho_w} \quad \text{and} \quad C = \frac{M_w}{\rho_w} \quad (5)$$

For a more detailed description of the procedure, see Rissler et al. (2004), Vestin et al. (2007) and Rissler et al. (2006). In Rissler et al. (2004), the soluble volume fraction, ε , was used instead of κ_R , otherwise the calculations were analogous.

By using the surface tension of water, the presence of surface active compounds is neglected. However, HULIS are suspected to act as surface active compounds, reducing the surface tension of water at the point of activation (Kiss et al., 2005). To get an estimate of the surface tension effect of HULIS, the surface tension was adjusted until the modelled supersaturation based on HTDMA derived growth factors was equal to the measured critical supersaturation. This was done for the HULIS sample from K-pusztá, where both CCNC and H-TDMA data was available. Note that a measurement or model error will result in an incorrect estimation of the surface tension.

4.3.2 ρ_{ion} model

The second model used in this work was first introduced by Ziese et al. (2007) for a similar HULIS sample set. It is also based on Köhler theory, but without taking into account the non-ideality of the solute. The growth factor from the H-TDMA data serves as input to the model to calculate the number of soluble entities per volume unit, here called ρ_{ion} , assuming a constant solubility and dissociation up into the supersaturated regime. The equation used to describe the water uptake is

$$S = \exp\left(\frac{4M_w\sigma}{RT\rho_w d_p} - \frac{\rho_{\text{ion}} \cdot M_w}{\rho_w} \frac{D_p^3}{D_{\text{drop}}^3 - D_p^3}\right) \quad (6)$$

where ρ_{ion} is defined as

$$\rho_{\text{ion}} = \frac{\nu \cdot \rho_s \cdot \phi}{M_s} \quad (7)$$

where ν is the maximum number of ions that the molecule can dissociate into and is the osmotic coefficient. Note that ρ_{ion} has the same meaning as κ_R , namely the number of moles of soluble material per dry particle volume. Equation (6) is in principle the Köhler equation, with an approximation made of dilute solutions (compare Eq. 17.24 in Seinfeld and Pandis, 2006). This is one more approximation compared to Eq. (3a), used in the κ_R model at subsaturations, but does not assume, as in the approximation used at super saturation, Eq. (4), that the volume occupied by the solute can be neglected relative to the droplet volume.

In the ρ_{ion} -model an additional variable is introduced; the surface tension is not held constant, or retrospectively adjusted to CCNC data one dry size at the time, but forced to follow the Szyszkowski-Langmuir equation (Szyszkowski, 1908):

$$\sigma = \sigma_w - aT \ln(1 + bC) \quad (8)$$

Title Page

Abstract

Introduction

Conclusions

References

Tables

Figures

⏪

⏩

◀

▶

Back

Close

Full Screen / Esc

Printer-friendly Version

Interactive Discussion

where σ_w is the surface tension of water, C is the number of moles of solute per mass of water and a and b are fitting parameters. Introducing a new parameter, b' , according to

$$b' = b \cdot \frac{\rho_s}{M_s \rho_w} \quad (9)$$

5 Eq. (8) can be rewritten as

$$\sigma = \sigma_w - aT \ln \left(1 + b' \frac{d_{p,0}^3}{d_p^3 - d_{p,0}^3} \right) \quad (10)$$

Equation (6) can now be rewritten as

$$S = \exp \left(\frac{4M_w \left(\sigma_w - aT \ln \left(1 + b' \frac{d_{p,0}^3}{d_p^3 - d_{p,0}^3} \right) \right)}{RT \rho_w d_p} - \frac{\rho_{\text{ion}} M_w}{\rho_w} \frac{d_{p,0}^3}{d_p^3 - d_{p,0}^3} \right) \quad (11)$$

10 An iteration procedure is then carried out to find a solution that matches both the CCNC and the H-TDMA data. As an initial guess, the surface tension is assumed to be the same as for water and can be calculated from Eq. (11), rearranged as

$$\rho_{\text{ion}} = \frac{\rho_w (d_p^3 - d_{p,0}^3)}{M_w d_{p,0}^3} \cdot \left(\frac{4M_w \left(\sigma_w - aT \ln \left(1 + b' \frac{d_{p,0}^3}{d_p^3 - d_{p,0}^3} \right) \right)}{RT \rho_w d_p} - \ln(S) \right) \quad (12)$$

15 based only on the Gf in one point from the H-TDMA data set. From Eq. (11), the critical supersaturation can now be calculated and the parameters a and b' , which define the surface tension of the sample, are adjusted until the result of the modelled critical supersaturation from the H-TDMA data matches the CCNC data. These parameters

Hygroscopic properties of Amazonian biomass burning

E. O. Fors et al.

Title Page

Abstract

Introduction

Conclusions

References

Tables

Figures

⏪

⏩

◀

▶

Back

Close

Full Screen / Esc

Printer-friendly Version

Interactive Discussion



are now used to calculate a new and the iteration continues until the solution has converged (Ziese et al. 2007).

The main advantage of this approach is that one obtains a concentration dependent surface tension function as an output, which is consistent with the Szyszkowski-Langmuir equation. The drawback is that no non-ideal behaviour between the water activity used for the H-TDMA measurement and the water activity at the activation point is taken into account, unlike the κ_R model, where the model salt is assumed to describe the non-ideality of the particle. It should also be noted that the surface tension parameters are adjusted until they match the data. A measurement error (or model error) will therefore result in an incorrect surface tension parameterization.

At subsaturation the ρ_{ion} model uses a more approximate form of the Köhler equation than the κ_R model. However, at supersaturations the formula is not using the assumption that the volume occupied by the solute can be neglected relative to the droplet volume as made in the κ_R model (Seinfeld and Pandis, 2006).

4.4 ZSR method

To estimate the relative volume parts of the HULIS and effluent part of the K-pusztá samples, the *Zdanovskii-Stokes-Robinson* method was used (Stokes and Robinson, 1966). At any specific water activity, the hygroscopic growth factor of the mixture, Gf_{mix} , can be written as

$$Gf_{mix} = \sqrt[3]{\sum \varepsilon_s Gf_s^3} \quad (13)$$

where ε_s are the volume fractions of the HULIS and the effluent in the dry particle, and Gf_s are the individual compounds' corresponding growth factors. In this work, Gf_s from the complete humidograms of the HULIS, the effluent and the extract samples were used as input to Eq. (13). For this, a single parameter function based on Köhler

Hygroscopic properties of Amazonian biomass burning

E. O. Fors et al.

Title Page

Abstract

Introduction

Conclusions

References

Tables

Figures

◀

▶

◀

▶

Back

Close

Full Screen / Esc

Printer-friendly Version

Interactive Discussion

theory was used to fit the H-TDMA data:

$$Gf = \sqrt[3]{1 + A \cdot \frac{RH/100}{1 - RH/100}} \quad (14)$$

where A is a fitting variable.

5 Results and discussion

5.1 Hygroscopic properties

The HULIS samples from both SMOCC and K-Pusztta showed low hygroscopic growth. The variability in diameter growth factors at 90% RH was quite small and fell in the range between 1.05 and 1.11 for all HULIS samples (Figs. 2 and 3 and Table 2). This is in the lower range of what has been reported previously by others (Gysel et al., 2004; Dinar et al., 2006; Ziese et al., 2007), where growth factors at 90% RH have been found to be between 1.05 and 1.24 (Table 2). In Table 3 the κ_R values are shown, calculated for the hygroscopic growth between 90–98% RH. The calculations were made both assuming a dissociation as that of a model salt (here Ammonium sulphate) and assuming full dissociation (values in parenthesis). For both SMOCC sampling periods, the day samples were more hygroscopic than the night samples. Figure 3 presents the humidograms for the two SMOCC periods, and for comparison, hygroscopic growth measured on-line at the SMOCC site during the time periods, averaged as internal mixture and weighted by mass (to simulate the soluble ions collected on a filter and re-suspended) is shown. As can be seen, the HULIS samples are significantly less hygroscopic than the on-site measurements, due to the absence of inorganic salts which are found the ambient aerosol but not in the isolated HULIS samples.

Determining the κ_R values for all HULIS samples revealed that they most often were dissolved and non-ideal to similar degrees throughout the RH range from 90 to 98%. The only exceptions are both SMOCC samples from period 3 (SMOCC D3 and N3),

26940

Hygroscopic properties of Amazonian biomass burning

E. O. Fors et al.

Title Page

Abstract

Introduction

Conclusions

References

Tables

Figures

⏪

⏩

◀

▶

Back

Close

Full Screen / Esc

Printer-friendly Version

Interactive Discussion



where an increase in the number of soluble entities per volume unit, κ_R , above 90% was observed with increased RH (Figs. 4 and 5, Table 3). Although these are the only HULIS samples in this work to show such behaviour, this effect has been observed previously for HULIS samples collected in Budapest (Ziese et al., 2007), and can possibly be explained by the presence of chemical compounds gradually dissolving as the RH increases. This behaviour makes a simple parameterization for CCN activity based on hygroscopicity at subsaturation a difficult task. It is also noteworthy that the K-pusztá winter samples (extract- and effluent samples) and the summer effluent sample also display this non-ideal behaviour (Fig. 4 and Table 3). This can be due to inorganic or organic compounds, that are present in both samples (recall that typically 40% of the HULIS was not extracted from the effluent sample), which take up water, and increase the dilution so that the HULIS will dissociate to a higher extent than in the isolated HULIS sample. Another interpretation is that inorganic salts with a high deliquescence point, such as K_2SO_4 , are present in the extract and effluent samples.

For the SMOCC samples, H-TDMA measurements were done both with humidification in the aerosol and the sheath air, and with constant pre-humidification to 90% in the aerosol line with subsequent RH control in the sheath air. This means that with the pre-humidification, the particles will have a possibility to deliquescent and restructure (restructuring decreases their mobility diameter) before equilibrating. This operating mode allowed measuring signs of efflorescence and restructuring of the aerosol. Both SMOCC night samples showed clear signs of restructuring, with Gf values below 1 at low RH, indicating shrinkage of the particles after the pre-humidification, while for the day samples this effect was less pronounced.

5.2 Cloud nucleating properties

As can be seen in Fig. 6 and Table 4, the critical supersaturations, s_c , experimentally determined for HULIS samples from the European rural background were significantly higher than for the water extract and the effluent samples, which is consistent with the hygroscopic growth measured at subsaturations. This result is not surprising,

Hygroscopic properties of Amazonian biomass burning

E. O. Fors et al.

Title Page

Abstract

Introduction

Conclusions

References

Tables

Figures

⏪

⏩

◀

▶

Back

Close

Full Screen / Esc

Printer-friendly Version

Interactive Discussion



considering that the hygroscopic inorganic salts and highly soluble organic compounds are contained in the water extract and the effluent. The small difference in s_c between the effluents and the extracts indicates that the HULIS in the European sample only weakly influence the point of activation. The critical supersaturations measured by the CCNC for the SMOCC samples are presented in Table 4 and Fig. 9. The measured s_c values were in the same range as in the European HULIS winter sample, although the SMOCC day sample (SMOCC D2) was found slightly less hygroscopic.

5.3 Comparison CCN measurements and model results

For the modelling of critical supersaturations, average values of κ_R and ρ_{ion} calculated from H-TDMA data between 95 and 98% RH were used. Both models were tested at first using the surface activity of pure water and the resulting critical supersaturation was compared to that measured. For the extract and effluent samples from K-Pusztá, the modelled and measured critical supersaturations were in good agreement, with a slightly overestimated s_c , explained by the droplet surface tension likely being somewhat lower than that of pure water. However, using the surface tension of pure water in the calculations for the K-pusztá HULIS sample leads to a clear overestimation of the critical supersaturation, which means that the HULIS activate more easily in the CCN counter than predicted by the model calculations (Fig. 7a and b). This is consistent with previous findings that HULIS can lower the surface tension, and thereby reduce the critical supersaturation (Graber et al., 2006). For a surface tension of water, both models overestimate the critical supersaturation by a factor of ~ 2 .

The ρ_{ion} and the κ_R model showed quite similar results. This is the case even though the non ideal behaviour is considered in the κ_R model, which is explained by that the correction term (χ_φ) at sub saturation and at activation is nearly the same, and therefore the effect of taking the non ideal behaviour into account is minor. For the HULIS sample, the ρ_{ion} model gives a lower s_c value than the κ_R model. This difference originates mainly from the different degrees of simplifications included in

Hygroscopic properties of Amazonian biomass burning

E. O. Fors et al.

[Title Page](#)[Abstract](#)[Introduction](#)[Conclusions](#)[References](#)[Tables](#)[Figures](#)[⏪](#)[⏩](#)[◀](#)[▶](#)[Back](#)[Close](#)[Full Screen / Esc](#)[Printer-friendly Version](#)[Interactive Discussion](#)

**Hygroscopic properties of
Amazonian biomass
burning**E. O. Fors et al.

[Title Page](#)[Abstract](#)[Introduction](#)[Conclusions](#)[References](#)[Tables](#)[Figures](#)[⏪](#)[⏩](#)[◀](#)[▶](#)[Back](#)[Close](#)[Full Screen / Esc](#)[Printer-friendly Version](#)[Interactive Discussion](#)

the Köhler equations used to calculate the activation. In the predictions of the critical supersaturation based on the κ_R model, the solute volume is assumed to be small enough to be neglected at droplet activation, while the ρ_{ion} model does not make this assumption. Under normal circumstances, such as measurements using ambient aerosols, this effect will not be crucial, but it becomes significant when investigating compounds with growth factors similar to those of HULIS, as can be seen from the difference in critical supersaturation predicted by the two models. This effect and its dependence on measured Gf and dry size is illustrated in Fig. 8, where the predicted supersaturations for 50 and 100 nm dry particles are presented as a function of measured Gf at 90% RH. When the hygroscopic growth approaches 1 (hydrophobic particles), the s_c values should converge towards the theoretical value of the Kelvin effect. This is the case for the ρ_{ion} model, while the κ_R approach overpredicts the s_c values. Based on this fact, the κ_R approach should not be used for predicting s_c values from Gf values close to 1, without taking this into account. In the two studies by Rissler et al. (2004) and Vestin et al. (2007) this effect was corrected for.

To determine the surface tension effect of the K-pusztas samples, the iteration procedure described in a previous section was carried out to derive the Szyszkowski surface tension parameterization. This approach also affects the estimation of ρ_{ion} from the hygroscopic growth at subsaturations. The results are presented in Tables 5 and 6. For the HULIS sample, this reveals a value of $\rho_{ion}=1157$ moles/m³ which is lower than reported previously (between 3516 moles/m³ and 13 269 moles/m³) in similar studies (Ziese et al., 2007). As can be seen in Table 5, for the ρ_{ion} procedure, the surface tension at activation of the HULIS sample was estimated to be between 47.7 mN/m for 50 nm dry size particles and 50.3 mN/m for 120 nm dry size particles.

The iteration procedure was also carried out for the winter and summer extract and the winter and summer effluent samples. In all cases, the iteration calculation converged towards a solution. According to the model, all samples, to different degrees, showed surface tensions lower than that of pure water at the point of activation (Table 5). The surface tension lowering of the effluent samples were less pronounced

than the extract samples. This can be expected since the extract samples include both the inorganic compounds and the full HULIS fraction, while the effluent samples include the inorganic compounds but only the part of the HULIS fraction that was not retained in the SPE column (Varga, 2001).

For the κ_R model a similar procedure was used, adjusting σ for each dry size individually until the residual between the modelled and the measured s_c was minimized. The κ_R model gave a similar but slightly lower σ at cloud droplet activation than the ρ_{ion} procedure with surface tensions at activation, ranging between 43.7 mN/m for 50 nm dry size particles and 47.2 nN/m for 100 nm dry size particles for the K-pusztá winter HULIS samples. The different results for the two models are explained by the overestimation of the supersaturation in the κ_R model previously discussed. In any case, these results indicate that the rural HULIS discussed in this work is more surface active than the urban HULIS previously investigated by Ziese et al. (2007), which gave σ values for HULIS between 52.1 mN/m (dry diameter 40.6 nm) and 70.3 mN/m (dry diameter 125 nm). The reason for this behaviour remains unknown.

The effect of surface active compounds is also dependent on the degree of external mixing. During the SMOCC campaign, H-TDMA measurements were done during the dry period, which confirmed the aerosol to be externally mixed, with two fractions having Gfs of 1.09 and 1.26 at 90% RH, respectively (Rissler et al., 2006). If the nearly hydrophobic mode consists of a large fraction of HULIS, the surface tension effect might actually have a substantial influence on cloud droplet activation, even though it is not evident in our internally mixed samples. ZSR modelling of the H-TDMA data suggested that the HULIS fraction was larger for the winter sample, with a volume fraction of the water soluble species, i.e. the extract sample, of $\sim 36\%$ compared to the summer sample, where it was $\sim 21\%$. It can be assumed that the concentration of HULIS originating from natural biological sources will be significantly lower during winter. However, this does not necessarily mean that the volume ratio between inorganics and HULIS will change accordingly, since this ratio is also influenced by combustion particles, which contribute inorganic ions, but which also may contribute to the HULIS

Hygroscopic properties of Amazonian biomass burning

E. O. Fors et al.

Title Page

Abstract

Introduction

Conclusions

References

Tables

Figures

⏪

⏩

◀

▶

Back

Close

Full Screen / Esc

Printer-friendly Version

Interactive Discussion

fraction via oxidation of soot. Total concentration measurements would be needed to draw further conclusions on this matter.

For the SMOCC samples, it is not possible to draw very far-reaching conclusions, since the H-TDMA measurements were carried out before and after the CCNC measurements, and not at the same time. This means that a closure based on CCNC and H-TDMA measurements will use different sample periods for the different instruments, and changes in e.g. air mass origin will have an effect on the closure. However, when using the ρ_{ion} approach on the H-TDMA data using the surface tension of water, the critical supersaturation was overpredicted for all instances except the SMOCC D3 sample, again indicating that the HULIS in these samples could also affect the surface tension (Fig. 9a and b).

As a final remark, it should be noted that possible bulk to surface partitioning effects such as described by Prisle et al. (2008) have not been taken into account. To our knowledge there is no current way of quantifying this effect for a mixed particle of unknown chemical composition.

For the growing droplet, this surface partitioning will result in a lower number of soluble entities in the bulk compared to a bulk system with the same overall chemical composition. The surface-to-bulk ratio decreases with increased water uptake and may lead to a migration of surface active compounds from the surface to the bulk. When extrapolating data from subsaturation to supersaturation without taking this into account, Raoult's law (the "salt" effect) is underestimated, leading to an overprediction of the critical supersaturation. Since compounds that have this behaviour are surface active, they may also lower the surface tension, leading to additional overprediction of the critical supersaturation. This means that our iterated surface tension values can be considered lower limit values, since they are calculated assuming no surface to bulk partitioning.

Hygroscopic properties of Amazonian biomass burning

E. O. Fors et al.

Title Page

Abstract

Introduction

Conclusions

References

Tables

Figures



Back

Close

Full Screen / Esc

Printer-friendly Version

Interactive Discussion



6 Summary and conclusions

We investigated HULIS samples with two different origins: aged biomass burning aerosol from Brazil (SMOCC sample) and rural Hungarian aerosol (K-Pusztasample). Their hygroscopic properties were determined using H-TDMA and CCNC techniques, and two different models were used to parameterize the Köhler equation from the sub-saturated H-TDMA data to predict the supersaturation at the point of activation. Furthermore, for the rural Hungarian aerosol samples, the total soluble fraction (extracts) and the fraction remaining after removing the HULIS from the extracts (effluents) were analysed.

The six HULIS samples showed hygroscopic growth factors between 1.05 and 1.11 for 100 nm particles at 90% RH. The models successfully predicted the critical supersaturations of the extract- and the effluent samples when assuming that the particles had the surface tension of pure water. The critical supersaturations of HULIS particles were overpredicted by between 0.9% (absolute) for the 50 nm dry size and 0.3% for the 120 nm dry size when assuming water surface tension. The difference between the response of 50 and 120 nm particles is to be expected, as small particles are more sensitive to changes in surface tension. When iteratively adjusting the surface tension to minimize the residual between the CCNC and the H-TDMA data, surface tensions at the point of activation were found between 47.7 and 50.3 mN/m for dry sizes between 50 and 120 nm, which is a significant decrease from the surface tension of water (72.8 mN/m). A moderate lowering of the effluent and extract samples' surface tensions was observed, indicating that the effect may have an influence on the ambient aerosol. However, the effect on critical supersaturation was minor.

All SMOCC HULIS samples showed similar hygroscopic properties compared to the Hungarian HULIS sample, with the day samples showing slightly lower hygroscopicity. Since the biomass burning samples were either analysed with the H-TDMA or the CCNC, and not in parallel due to a lack of sample volume, it is not possible to draw definite conclusions from these samples. However, predictions of the critical

Hygroscopic properties of Amazonian biomass burning

E. O. Fors et al.

Title Page

Abstract

Introduction

Conclusions

References

Tables

Figures

⏪

⏩

◀

▶

Back

Close

Full Screen / Esc

Printer-friendly Version

Interactive Discussion

supersaturation from the average hygroscopic growth factors (from four samples) using water surface tension seem to overestimate the measured critical supersaturation. This also suggests that the surface tension at the point of activation is lower than that of water due to the HULIS' surfactant properties.

5 It can be concluded that HULIS can have a significant surface activity potential when isolated, and this alters the critical supersaturation needed for activation of cloud droplets. However, when they act as part of the entire water soluble matter, this effect is no longer significant, most likely due to the water uptake by inorganic salts, which have a high solubility and dilutes the HULIS concentration. In this study only
10 one HULIS measurement could be used to draw a quantitative conclusion regarding this effect, and given the diversity of different kinds of HULIS which are available in the atmosphere, more general conclusions would need further investigation on the matter.

Acknowledgement. This work was carried out within the framework of Smoke, Aerosols, Clouds, Rainfall, and Climate (SMOCC) project, a European contribution to the Large-Scale Biosphere-Atmosphere Experiment in Amazonia (LBA). It was financially supported by the
15 Environmental and Climate Program of the European Commission (contract EVK-2-CT-2001-00110 SMOCC). The authors would also like to thank the Swedish Research Council, and the Danish Natural Science Research Council.

References

- 20 Andreae, M. O. and Rosenfeld, D.: Aerosol-cloud-precipitation interactions. Part 1. The nature and sources of cloud-active aerosols, *Earth Sci. Rev.*, 89, 13–41, 2008.
- Bilde, M. and Svenningsson, B.: CCN activation of slightly soluble organics: the importance of small amounts of inorganic salt and particle phase, *Tellus B*, 56(2), 128–134, 2004.
- Charlson, R. J., Seinfeld, J. H., Nenes, A., Kulmala, M., Laaksonen, A., and Facchini, C., F.:
25 Atmospheric science – Reshaping the theory of cloud formation, *Science*, 292(5524), 2025–2026, 2001.
- Decesari, S., Facchini, M. C., Matta, E., Mircea, M., Fuzzi, S., Chughtai, A. R., and Smith, D. M.:

Hygroscopic properties of Amazonian biomass burning

E. O. Fors et al.

Title Page

Abstract

Introduction

Conclusions

References

Tables

Figures

◀

▶

◀

▶

Back

Close

Full Screen / Esc

Printer-friendly Version

Interactive Discussion

Water soluble organic compounds formed by oxidation of soot, *Atmos. Environ.*, 36, 1827–1832, 2002.

Decesari, S., Fuzzi, S., Facchini, M. C., Mircea, M., Emblico, L., Cavalli, F., Maenhaut, W., Chi, X., Schkolnik, G., Falkovich, A., Rudich, Y., Claeys, M., Pashynska, V., Vas, G., Kourtchev, I., Vermeylen, R., Hoffer, A., Andreae, M. O., Tagliavini, E., Moretti, F., and Artaxo, P.: Characterization of the organic composition of aerosols from Rondônia, Brazil, during the LBA-SMOCC 2002 experiment and its representation through model compounds, *Atmos. Chem. Phys.*, 6, 375–402, 2006,
<http://www.atmos-chem-phys.net/6/375/2006/>.

Dinar, E., Taraniuk, I., Graber, E. R., Katsman, S., Moise, T., Anttila, T., Mentel, T. F., and Rudich, Y.: Cloud Condensation Nuclei properties of model and atmospheric HULIS, *Atmos. Chem. Phys.*, 6, 2465–2482, 2006,
<http://www.atmos-chem-phys.net/6/2465/2006/>.

Facchini, M. C., Decesari, S., Mircea, M., Fuzzi, S., and Loglio, G.: Surface tension of atmospheric wet aerosol and cloud/fog droplets in relation to their organic carbon content and chemical composition, *Atmos. Environ.*, 34(28), 4853–4857, 2000.

Frank, G. P., Dusek, U., and Andreae, M. O.: Technical Note: Characterization of a static thermal-gradient CCN counter, *Atmos. Chem. Phys.*, 7, 3071–3080, 2007,
<http://www.atmos-chem-phys.net/7/3071/2007/>.

Fuzzi, S., Decesari, S., Facchini, M. C., Cavalli, F., Emblico, L., Mircea, M., Andreae, M. O., Trebs, I., Hoffer, A., Guyon, P., Artaxo, P., Rizzo, L. V., Lara, L. L., Pauliquevis, T., Maenhaut, W., Raes, N., Chi, X. G., Mayol-Bracero, O. L., Soto-Garcia, L. L., Claeys, M., Kourtchev, I., Rissler, J., Swietlicki, E., Tagliavini, E., Schkolnik, G., Falkovich, A. H., Rudich, Y., Fisch, G., and Gatti, L. V.: Overview of the inorganic and organic composition of size-segregated aerosol in Rondonia, Brazil, from the biomass-burning period to the onset of the wet season, *J. Geophys. Res.-Atmos.*, 112, D01201, doi:10.1029/2005JD006741, 2007.

Gelencser, A., Hoffer, A., Krivacsy, Z., Kiss, G., Molnar, A., and Meszaros, E.: On the possible origin of humic matter in fine continental aerosol, *J. Geophys. Res.-Atmos.*, 107(D12), 4137, doi:10.1029/2001JD001299, 2002.

Graber, E. R. and Rudich, Y.: Atmospheric HULIS: How humic-like are they? A comprehensive and critical review, *Atmos. Chem. Phys.*, 6, 729–753, 2006,
<http://www.atmos-chem-phys.net/6/729/2006/>.

ACPD

9, 26925–26967, 2009

Hygroscopic properties of Amazonian biomass burning

E. O. Fors et al.

Title Page

Abstract

Introduction

Conclusions

References

Tables

Figures

⏪

⏩

◀

▶

Back

Close

Full Screen / Esc

Printer-friendly Version

Interactive Discussion

Hygroscopic properties of Amazonian biomass burningE. O. Fors et al.

[Title Page](#)[Abstract](#)[Introduction](#)[Conclusions](#)[References](#)[Tables](#)[Figures](#)[⏪](#)[⏩](#)[◀](#)[▶](#)[Back](#)[Close](#)[Full Screen / Esc](#)[Printer-friendly Version](#)[Interactive Discussion](#)

- Gysel, M., Weingartner, E., Nyeki, S., Paulsen, D., Baltensperger, U., Galambos, I., and Kiss, G.: Hygroscopic properties of water-soluble matter and humic-like organics in atmospheric fine aerosol, *Atmos. Chem. Phys.*, 4, 35–50, 2004, <http://www.atmos-chem-phys.net/4/35/2004/>.
- 5 Jacobson, M. C., Hansson, H. C., Noone, K. J., and Charlson, R. J.: Organic atmospheric aerosols: Review and state of the science, *Rev. Geophys.*, 38, 267–294, 2000.
- Kaufman, Y. J., Tanre, D., and Boucher, O.: A satellite view of aerosols in the climate system, *Nature*, 419, 215–223, 2002.
- Kanakidou, M., Seinfeld, J. H., Pandis, S. N., Barnes, I., Dentener, F. J., Facchini, M. C., Van Dingenen, R., Ervens, B., Nenes, A., Nielsen, C. J., Swietlicki, E., Putaud, J. P., Balkanski, Y., Fuzzi, S., Horth, J., Moortgat, G. K., Winterhalter, R., Myhre, C. E. L., Tsigaridis, K., Vignati, E., Stephanou, E. G., and Wilson, J.: Organic aerosol and global climate modelling: a review, *Atmos. Chem. Phys.*, 5, 1053–1123, 2005, <http://www.atmos-chem-phys.net/5/1053/2005/>.
- 15 Kiss, G., Tombacz, E., and Hansson, H.-C.: Surface tension effects of humic-like substances in the aqueous extract of tropospheric fine aerosol, *J. Atmos. Chem.*, 50, 279–294, 2005.
- Kleefeld, S., Hoffer, A., Krivacsy, Z., and Jennings, S. G.: Importance of organic and black carbon in atmospheric aerosols at Mace Head, on the West Coast of Ireland (53°19' N, 9°54' W), *Atmos. Environ.*, 36, 4479–4490, 2002.
- 20 Kreidenweis, S. M., Koehler, K., DeMott, P. J., Prenni, A. J., Carrico, C., and Ervens, B.: Water activity and activation diameters from hygroscopicity data – Part I: Theory and application to inorganic salts, *Atmos. Chem. Phys.*, 5, 1357–1370, 2005, <http://www.atmos-chem-phys.net/5/1357/2005/>.
- Krivacsy, Z., Hoffer, A., Sarvari, Z., Temesi, D., Baltensperger, U., Nyeki, S., Weingartner, E., Kleefeld, S., and Jennings, S. G.: Role of organic and black carbon in the chemical composition of Atmospheric aerosol at European background sites, *Atmos. Environ.*, 35, 6231–6244, 2001.
- 25 Limbeck, A., Kulmala, M., and Puxbaum, H.: Secondary organic aerosol formation in the atmosphere via heterogeneous reaction of gaseous isoprene on acidic particles, *Geophys. Res. Lett.*, 30(19), 1996, doi:10.1029/2003GL017738, 2003.
- 30 Low, R. D. H.: A theoretical study of nineteen condensation nuclei, *J. Res. Atmos.*, 4, 65–78, 1969.
- Mayol-Bracero, O. L., Guyon, P., Graham, B., Roberts, G., Andreae, M. O., Decesari, S.,

Facchini, M. C., Fuzzi, S., and Artaxo, P.: Water-soluble organic compounds in biomass burning aerosols over Amazonia – 2. Apportionment of the chemical composition and importance of the polyacidic fraction, *J. Geophys. Res.-Atmos.*, 107, D208091, doi:10.1029/2001JD000522, 2002.

5 Nenes, A., Charlson, R. J., Facchini, M. C., Kulmala, M., Laaksonen, A., and Seinfeld, J. H.: Can chemical effects on cloud droplet number rival the first indirect effect?, *Geophys. Res. Lett.*, 29(17), 1848, doi:10.1029/2002GL015295, 2002.

Petters, M. D. and Kreidenweis, S. M.: A single parameter representation of hygroscopic growth and cloud condensation nucleus activity, *Atmos. Chem. Phys.*, 7, 1961–1971, 2007, <http://www.atmos-chem-phys.net/7/1961/2007/>.

10 Pio, C. A., Legrand, M., Oliveira, T., Afonso, J., Santos, C., and Caseiro, A.: Climatology of aerosol composition (organic versus inorganic) at non-urban sites on a west-east transect across Europe, *J. Geophys. Res.*, 112, D23S02, doi:10.1029/2006JD008038, 2007.

Potukuchi, S. and Wexler, A. S.: Identifying solid–aqueous phase transitions in atmospheric aerosols: I. Neutral-acidity solutions, *Atmos. Environ.*, 29, 1663–1676, 1995.

15 Prisle, N. L., Raatikainen, T., Sorjamaa, R., Svenningson, B., Laaksonen, A. and Bilde, M.: Surfactant partitioning in cloud droplet activation: a study of C8, C10, C12 and C14 normal fatty acid sodium salts, *Tellus B*, 60(3), 416–431, 2007.

20 Prisle, N. L., Raatikainen, T., Laaksonen, A., and Bilde, M.: Surfactants in cloud droplet activation: mixed organic-inorganic particles, *Atmos. Chem. Phys. Discuss.*, 9, 24669–24715, 2009, <http://www.atmos-chem-phys-discuss.net/9/24669/2009/>.

Ramanathan, V., Crutzen, P. J., Kiehl, J. T., and Rosenfeld, D.: Aerosols, climate, and the hydrological cycle, *Science*, 294, 2119–2124, 2001.

25 Rader, D. J. and McMurry, P. H.: Application of the tandem differential mobility analyzer for studies of droplet growth or evaporation, *J. Aerosol Sci.*, 17, 771–787, 1986.

Rissler, J., Swietlicki, E., Zhou, J., Roberts, G., Andreae, M. O., Gatti, L. V., and Artaxo, P.: Physical properties of the sub-micrometer aerosol over the Amazon rain forest during the wet-to-dry season transition - comparison of modeled and measured CCN concentrations, *Atmos. Chem. Phys. Discuss.*, 4, 3159–3225, 2004, <http://www.atmos-chem-phys-discuss.net/4/3159/2004/>.

30 Rissler, J., Vestin, A., Swietlicki, E., Fisch, G., Zhou, J., Artaxo, P., and Andreae, M. O.: Size distribution and hygroscopic properties of aerosol particles from dry-season biomass burning

Hygroscopic properties of Amazonian biomass burning

E. O. Fors et al.

Title Page

Abstract

Introduction

Conclusions

References

Tables

Figures

◀

▶

◀

▶

Back

Close

Full Screen / Esc

Printer-friendly Version

Interactive Discussion

- in Amazonia, *Atmos. Chem. Phys.*, 6, 471–491, 2006,
<http://www.atmos-chem-phys.net/6/471/2006/>.
- Rosenfeld, D.: Industrial air pollution suppression of rain and snow by urban and industrial air pollution, *Science*, 287, 1793, doi:10.1126/science.287.5459.1793, 2000.
- 5 Satheesh, S. K. and Moorthy, K. K.: Radiative effects of natural aerosols: A review, *Atmos. Environ.*, 39, 2089–2110, 2005.
- Seinfeld, J. H. and Pandis, S. N.: *Atmospheric Chemistry and Physics – From Air Pollution to Climate Change*, 2nd edition, Wiley Interscience, 2006.
- Snider, J. R. and Brenguier, J.-E.: Cloud condensation nuclei and cloud droplets during ACE-2,
10 *Tellus B*, 52, 828–842, 1999.
- Svenningsson, B., Rissler, J., Swietlicki, E., Mircea, M., Bilde, M., Facchini, M. C., Decesari, S., Fuzzi, S., Zhou, J., Mønster, J., and Rosenørn, T.: Hygroscopic growth and critical supersaturations for mixed aerosol particles of inorganic and organic compounds of atmospheric relevance, *Atmos. Chem. Phys.*, 6, 1937–1952, 2006,
15 <http://www.atmos-chem-phys.net/6/1937/2006/>.
- Sorjamaa, R., Svenningsson, B., Raatikainen, T., Henning, S., Bilde, M., and Laaksonen, A.: The role of surfactants in Köhler theory reconsidered, *Atmos. Chem. Phys.*, 4, 2107–2117, 2004,
<http://www.atmos-chem-phys.net/4/2107/2004/>.
- 20 Stokes, R. H. and Robinson, R. A.: Interactions in aqueous nonelectrolyte solutions, I. Solute-solvent equilibria, *J. Phys. Chem.*, 70, 2126–2131, 1966.
- Swietlicki, E., Zhou, J., Berg, O. H., Martinsson, B. G., Frank, G., Cederfelt, S.-I., Dusek, U., Berner, A., Birmili, W., Wiedensohler, A., Yuskiewicz, B., and Bower, K. N.: A closure study of sub-micrometer aerosol particle hygroscopic behavior, *Atmos. Res.*, 50, 205–240, 1999.
- 25 Swietlicki, E., Hansson, H.-C., Hämeri, K., Massling, A., Petäjä, T., Tunved, P., Weingartner, E., Baltensperger, U., McMurry, P. H., McFiggans, G., Svenningsson, B., Rissler, J., Wiedensohler, A., and Kulmala, M.: Hygroscopic properties of sub-micrometer atmospheric aerosol particles measured with H-TDMA instruments in various environments – a review, *Tellus B*, 60(3), 353–364, 2007.
- 30 Tang, I. N. and Munkelwitz, H. R.: Water activities, densities and refractive-indexes of aqueous sulfates and sodium-nitrate droplets of atmospheric importance, *J. Geophys. Res.*, 99, 18801–18808, 1999.
- Varga, B., Kiss, G., Ganszky, I., Gelencsér, A., and Krivácsy, Z.: Isolation of water-soluble

Hygroscopic properties of Amazonian biomass burning

E. O. Fors et al.

[Title Page](#)[Abstract](#)[Introduction](#)[Conclusions](#)[References](#)[Tables](#)[Figures](#)[◀](#)[▶](#)[◀](#)[▶](#)[Back](#)[Close](#)[Full Screen / Esc](#)[Printer-friendly Version](#)[Interactive Discussion](#)

- organic matter from atmospheric aerosol, *Talanta*, 55(3), 561–572, 2001.
- Vestin, A., Rissler, J., Swietlicki, E., Frank, G. P., and Andreae, M. O.: Cloud-nucleating properties of the Amazonian biomass burning aerosol: Cloud condensation nuclei measurements and modelling, *J. Geophys. Res.*, 112, D14201, doi:10.1029/2006JD008104, 2007.
- 5 Warner, J.: A reduction of rain associated with smoke from sugar-cane fires – An inadvertent weather modification, *J. Appl. Meteorol.*, 7, 247–251, 1968.
- Yang, H., Xu, J., Wu, W.-S., Wan, C. H., and Yu, J. Z.: Chemical characteristics of water-soluble organic aerosols at Jeju Island collected during ACE-Asia, *Environ. Chem.*, 1, 13–17, 2004.
- 10 Young, K. C. and Warren, A. J.: A reexamination of the derivation of the equilibrium supersaturation curve for soluble particles, *J. Atmos. Sci.*, 49, 1138–1143, 1992.

ACPD

9, 26925–26967, 2009

**Hygroscopic
properties of
Amazonian biomass
burning**

E. O. Fors et al.

Title Page

Abstract

Introduction

Conclusions

References

Tables

Figures

⏪

⏩

◀

▶

Back

Close

Full Screen / Esc

Printer-friendly Version

Interactive Discussion

Hygroscopic properties of Amazonian biomass burning

E. O. Fors et al.

Table 1. Origin of aerosol samples analyzed with the H-TDMA and the CCNC techniques.

Sample	Location	Sampling time	Type	Method used	
				H-TDMA	CCNC
HULIS (SMOCC, D1)	Rondônia, Brazil	Day, 17–21 Sep 2002	biomass burning	x	
HULIS (SMOCC, D2)	Rondônia, Brazil	Day, 21–28 Sep 2002	biomass burning		x
HULIS (SMOCC, D3)	Rondônia, Brazil	Day, 28 Sep–4 Oct 2002	biomass burning	x	
HULIS (SMOCC, N1)	Rondônia, Brazil	Night, 17–21 Sep 2002	biomass burning	x	
HULIS (SMOCC, N2)	Rondônia, Brazil	Night, 21–28 Sep 2002	biomass burning		x
HULIS (SMOCC, N3)	Rondônia, Brazil	Night, 28 Sep–4 Oct 2002	biomass burning	x	
Extract (Winter)	K-pusztá, Hungary	Day/Night, 16 Feb 2001	rural background	x	x
Effluent (Winter)	K-pusztá, Hungary	Day/Night, 16 Feb 2001	rural background	x	x
HULIS (Winter)	K-pusztá, Hungary	Day/Night, 16 Feb 2001	rural background	x	x
Extract (Summer)	K-pusztá, Hungary	Day/Night, 11 Jul 2001	rural background	x	x
Effluent (Summer)	K-pusztá, Hungary	Day/Night, 11 Jul 2001	rural background	x	x
HULIS (Summer)	K-pusztá, Hungary	Day/Night, 11 Jul 2001	rural background	x	

[Title Page](#)
[Abstract](#)
[Introduction](#)
[Conclusions](#)
[References](#)
[Tables](#)
[Figures](#)
[Back](#)
[Close](#)
[Full Screen / Esc](#)
[Printer-friendly Version](#)
[Interactive Discussion](#)

Hygroscopic properties of Amazonian biomass burning

E. O. Fors et al.

[Title Page](#)[Abstract](#)[Introduction](#)[Conclusions](#)[References](#)[Tables](#)[Figures](#)[⏪](#)[⏩](#)[◀](#)[▶](#)[Back](#)[Close](#)[Full Screen / Esc](#)[Printer-friendly Version](#)[Interactive Discussion](#)

Table 2. Previously measured HULIS growth factors at 90% RH together with the G_f from this work. Sample notations are according to the published papers.

Sample	G_f at 90% RH
KP010112-ISOM, 100 nm dry size (Gysel et al., 2004)	1.08
KP010126-ISOM, 100 nm dry size (Gysel et al., 2004)	1.11
KP010726-ISOM, 100 nm dry size (Gysel et al., 2004)	1.16
KP010816-ISOM, 100 nm dry size (Gysel et al., 2004)	1.17
LBO-night, 60 nm dry size (Dinar et al., 2006)	1.18
LBO-day, 60 nm dry size (Dinar et al., 2006)	1.24
Budapest, sample 1 (Ziese et al., 2007)	1.17
Budapest, sample 2 (Ziese et al., 2007)	1.05
K-pusztá, summer	1.11
K-pusztá, winter	1.05
SMOCC, D1	1.06
SMOCC, D3	1.11
SMOCC, N1	1.06
SMOCC, N3	1.05

Hygroscopic properties of Amazonian biomass burning

E. O. Fors et al.

Table 3. κ_R value statistics for RH values between 90 and 98%. The κ_R presented are based on assuming that the non-ideality of the solute can be accounted for by a model salt. κ_R values in paranthesis are values resulting from ideal behaviour or the droplet – assuming full dissociation. r^2 is the coefficient of determination between RH and κ_R . The significances of the trend (linear increase of κ_R as a function of RH) was also calculated (Trend 95% CI).

KAPPA values above 90% RH (moles/m ³)	average	std	r^2	Trend 95% CI
HULIS (K-puszt, winter)	1571 (1177)	179 (110)	0.09	NO
Effluent (K-puszt, winter)	16 777 (11 475)	2696 (1758)	0.82	YES
Extract (K-puszt, winter)	10 968 (7570)	2107 (1466)	0.83	YES
HULIS (K-puszt, summer)	2924 (2148)	482 (347)	0.02	NO
Effluent (K-puszt, summer)	22 584 (14 977)	994 (496)	0.67	YES
Extract (K-puszt, summer)	19 233 (12 844)	1517 (880)	0.62	NO
HULIS (SMOCC, D1)	2102 (1574)	134 (126)	0.03	NO
HULIS (SMOCC, D3)	4729 (3365)	680 (527)	0.89	YES
HULIS (SMOCC, N1)	1605 (1222)	1661 (168)	0.23	NO
HULIS (SMOCC, N3)	2604 (1910)	381 (347)	0.70	YES

Title Page

Abstract

Introduction

Conclusions

References

Tables

Figures

◀

▶

◀

▶

Back

Close

Full Screen / Esc

Printer-friendly Version

Interactive Discussion

Hygroscopic properties of Amazonian biomass burning

E. O. Fors et al.

Table 4. Critical supersaturation measured with the CCNCs for different dry diameters for samples from K-pusztá and SMOCC.

Dry diameter (nm)	Critical supersaturation (%)							
	40	50	60	75	80	100	120	125
Extract (K-pusztá, summer)	0.84	0.60	0.43		0.29	0.20		
Effluent (K-pusztá, summer)	0.79	0.54	0.41		0.25	0.18		
Extract (K-pusztá, winter)	1.15	0.70	0.50		0.30	0.21		
Effluent (K-pusztá, winter)	1.07	0.69	0.51		0.33	0.24		
HULIS (K-pusztá, winter)		1.11	0.87		0.60	0.44	0.28	
HULIS (SMOCC, D2)		1.36		0.82		0.55		0.26
HULIS (SMOCC, N2)		1.09		0.52		0.28		

[Title Page](#)
[Abstract](#)
[Introduction](#)
[Conclusions](#)
[References](#)
[Tables](#)
[Figures](#)
[⏪](#)
[⏩](#)
[◀](#)
[▶](#)
[Back](#)
[Close](#)
[Full Screen / Esc](#)
[Printer-friendly Version](#)
[Interactive Discussion](#)

Hygroscopic properties of Amazonian biomass burning

E. O. Fors et al.

Table 5. Surface tensions at the point of activation according to the ρ_{ion} model for the K-puszta winter sample.

Diameter (nm)	Surface tension at activation (mN/m)					
	40	50	60	80	100	120
Effluent (K-puszta, winter), Surface tension at point of activation (mN/m)	70.9	71	71	71.1	71.2	
Extract (K-puszta, winter), Surface tension at point of activation (mN/m)	60.3	60.7	60.9	61.5	61.8	
HULIS (K-puszta, winter), Surface tension at point of activation (mN/m)		47.7	48.2	49	50	50.3
Effluent (K-puszta, summer), Surface tension at point of activation (mN/m)	66.7	67	67.3	67.6	67.9	
Extract (K-puszta, summer)Surface tension at point of activation (mN/m)	63.6	64	64.2	64.6	64.9	

[Title Page](#)
[Abstract](#)
[Introduction](#)
[Conclusions](#)
[References](#)
[Tables](#)
[Figures](#)
[Back](#)
[Close](#)
[Full Screen / Esc](#)
[Printer-friendly Version](#)
[Interactive Discussion](#)

Hygroscopic properties of Amazonian biomass burning

E. O. Fors et al.

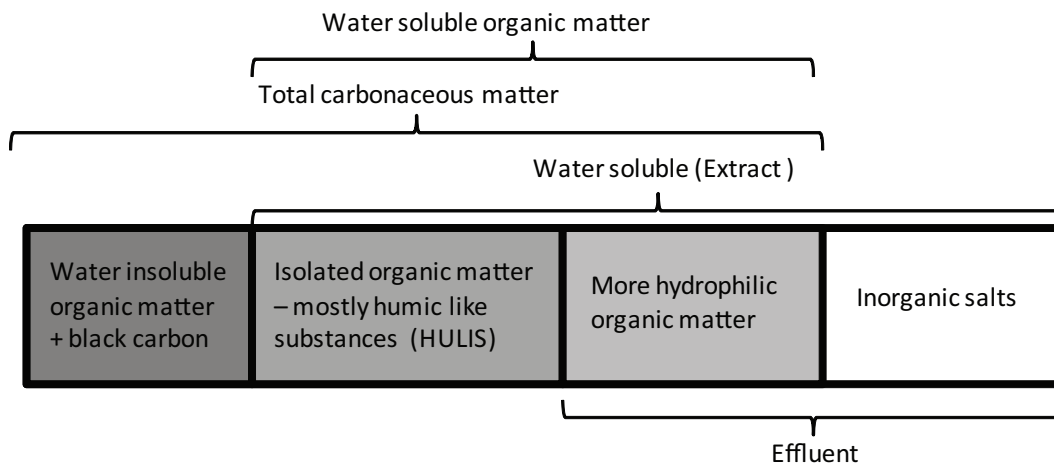
Table 6. Fitted parameters for the ρ_{ion} model for K-pusztá compared to previous calculations from Ziese et al. (2007). Note that ρ_{ion} is given using the fitted surface tensions while in Table 3 the corresponding numbers for the κ_{R} model are listed using the surface tension of pure water.

Substance	a (N/mK)	b'	ρ_{ion} (moles/m ³)
HULIS (K-pusztá, winter)	2.01×10^{-5}	10^6	1157
Effluent (K-pusztá, winter)	8.03×10^{-7}	10^6	12 692
Extract (K-pusztá, winter)	1.53×10^{-6}	10^6	8952
Effluent (K-pusztá, summer)	6.63×10^{-6}	10^6	15 552
Extract (K-pusztá, summer)	7.31×10^{-6}	10^6	12 105
HULIS, first sample, Budapest, Hungary (Ziese et al., 2007)	9.51×10^{-6}	10^2	5434
HULIS, second sample, Budapest, Hungary (Ziese et al., 2007)	2.14×10^{-5}	10^2	5268
HULIS, LBO night, Rehovot, Israel (Ziese et al., 2007)	3.51×10^{-5}	10^2	3516
HULIS, LBO day, Rehovot, Israel (Ziese et al., 2007)	3.57×10^{-5}	10^2	7317
HULIS, 3WSFA, Rehovot, Israel (Ziese et al., 2007)	2.68×10^{-5}	10^2	13 269

[Title Page](#)
[Abstract](#)
[Introduction](#)
[Conclusions](#)
[References](#)
[Tables](#)
[Figures](#)
[Back](#)
[Close](#)
[Full Screen / Esc](#)
[Printer-friendly Version](#)
[Interactive Discussion](#)

**Hygroscopic properties of
Amazonian biomass
burning**

E. O. Fors et al.

**Fig. 1.** Classification of a typical aerosol sample.[Title Page](#)[Abstract](#)[Introduction](#)[Conclusions](#)[References](#)[Tables](#)[Figures](#)[◀](#)[▶](#)[◀](#)[▶](#)[Back](#)[Close](#)[Full Screen / Esc](#)[Printer-friendly Version](#)[Interactive Discussion](#)

Hygroscopic properties of
Amazonian biomass
burning

E. O. Fors et al.

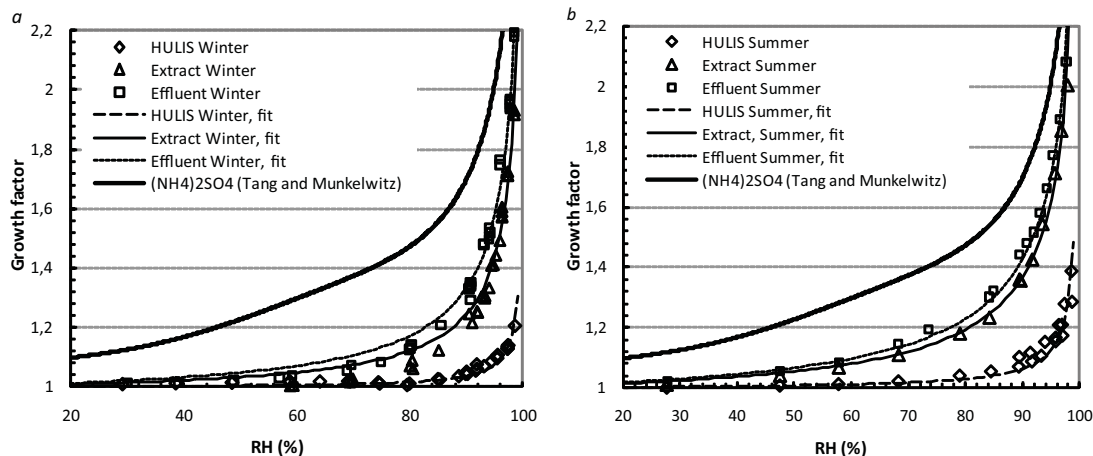


Fig. 2. Measured hygroscopic growth of Kpusza winter (a) and summer (b) samples and fitted functions for particles with a dry diameter of 100 nm. The solid line represents ammonium sulphate data from Tang and Munkelwitz (1999). The lines denoted *fit* are parameterisations according to Eq. (14).

[Title Page](#)[Abstract](#)[Introduction](#)[Conclusions](#)[References](#)[Tables](#)[Figures](#)[◀](#)[▶](#)[◀](#)[▶](#)[Back](#)[Close](#)[Full Screen / Esc](#)[Printer-friendly Version](#)[Interactive Discussion](#)

Hygroscopic properties of Amazonian biomass burning

E. O. Fors et al.

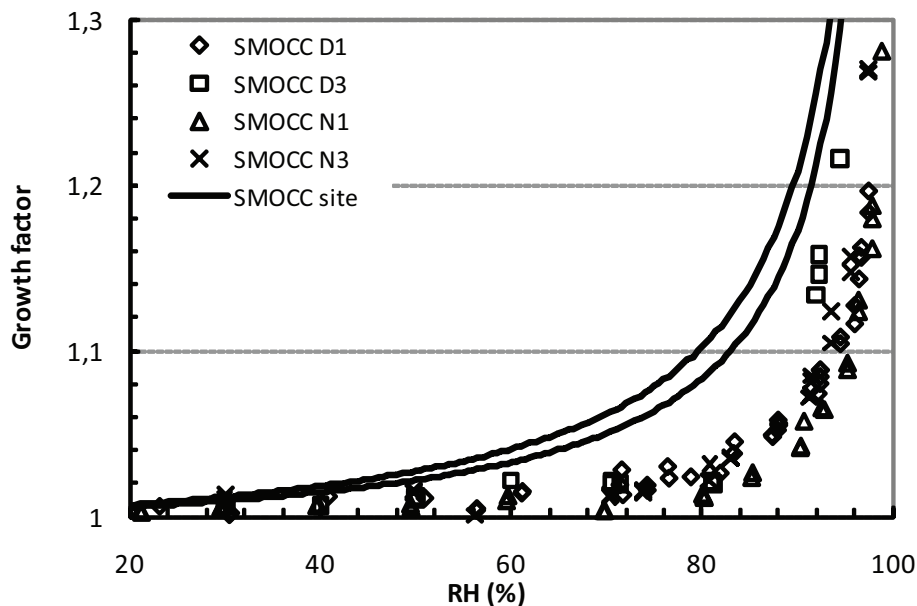


Fig. 3. Measured hygroscopic growth of 100 nm HULIS aerosol particles collected during the SMOCC campaign. The two SMOCC site parameterizations represent growth measured on site during the time periods, averaged as internal mixture and weighted by mass (to simulate the soluble ions collected on a filter and re-suspended). The average over all six periods ranges between the two solid lines.

Title Page

Abstract

Introduction

Conclusions

References

Tables

Figures

◀

▶

◀

▶

Back

Close

Full Screen / Esc

Printer-friendly Version

Interactive Discussion

**Hygroscopic properties of
Amazonian biomass
burning**

E. O. Fors et al.

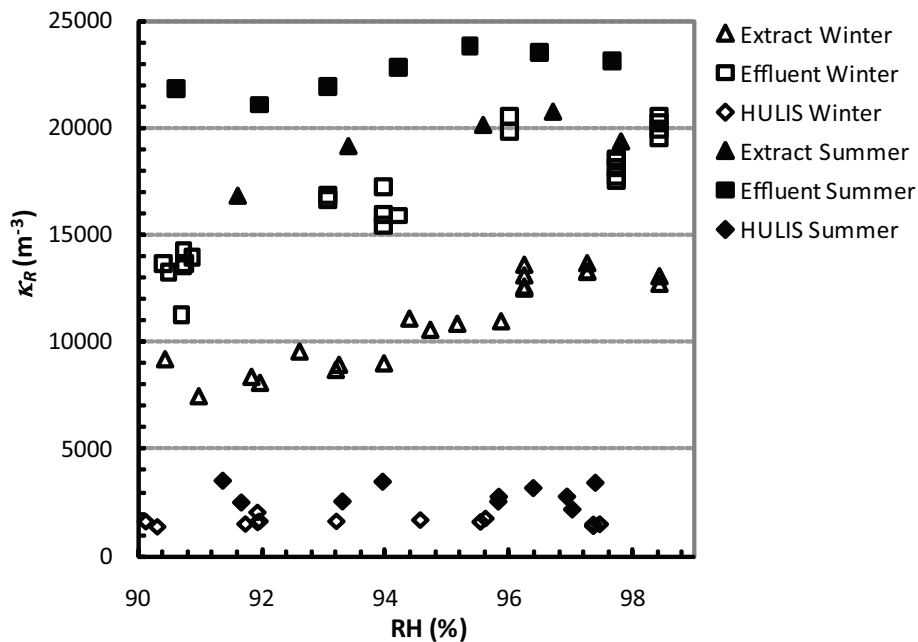


Fig. 4. κ_R for the K-pusztas samples calculated independently from Gf at all RH's.

[Title Page](#)[Abstract](#)[Introduction](#)[Conclusions](#)[References](#)[Tables](#)[Figures](#)[◀](#)[▶](#)[◀](#)[▶](#)[Back](#)[Close](#)[Full Screen / Esc](#)[Printer-friendly Version](#)[Interactive Discussion](#)

**Hygroscopic properties of
Amazonian biomass
burning**

E. O. Fors et al.

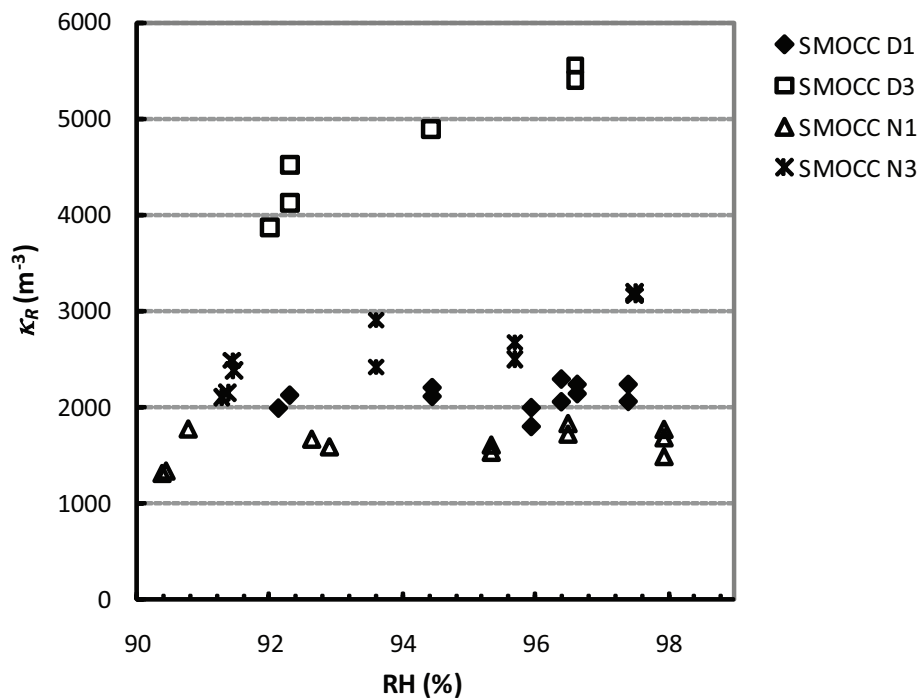


Fig. 5. κ_R for the SMOCC HULIS samples calculated independently from G_f at different RH's.

[Title Page](#)[Abstract](#)[Introduction](#)[Conclusions](#)[References](#)[Tables](#)[Figures](#)[◀](#)[▶](#)[◀](#)[▶](#)[Back](#)[Close](#)[Full Screen / Esc](#)[Printer-friendly Version](#)[Interactive Discussion](#)

**Hygroscopic properties of
Amazonian biomass
burning**

E. O. Fors et al.

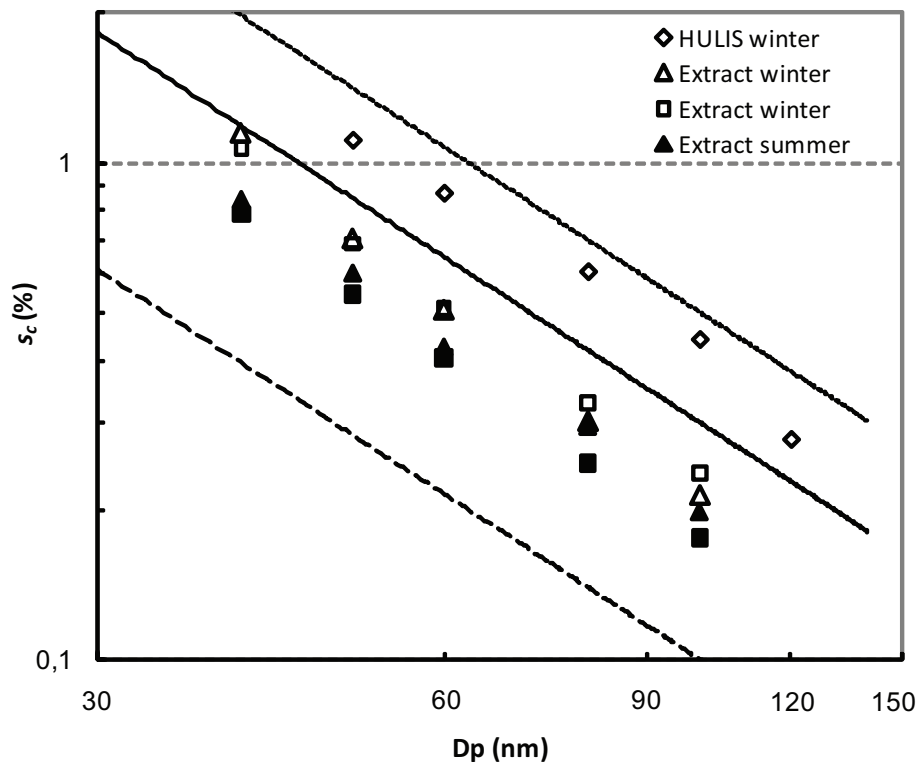


Fig. 6. Measured critical supersaturations for the K-pusztá samples. The lines represent the supersaturation ratios of three different arbitrary compounds as a function of dry diameter, D_p . The s_c values are calculated according to Eq. (4).

[Title Page](#)[Abstract](#)[Introduction](#)[Conclusions](#)[References](#)[Tables](#)[Figures](#)[◀](#)[▶](#)[◀](#)[▶](#)[Back](#)[Close](#)[Full Screen / Esc](#)[Printer-friendly Version](#)[Interactive Discussion](#)

Hygroscopic properties of Amazonian biomass burning

E. O. Fors et al.

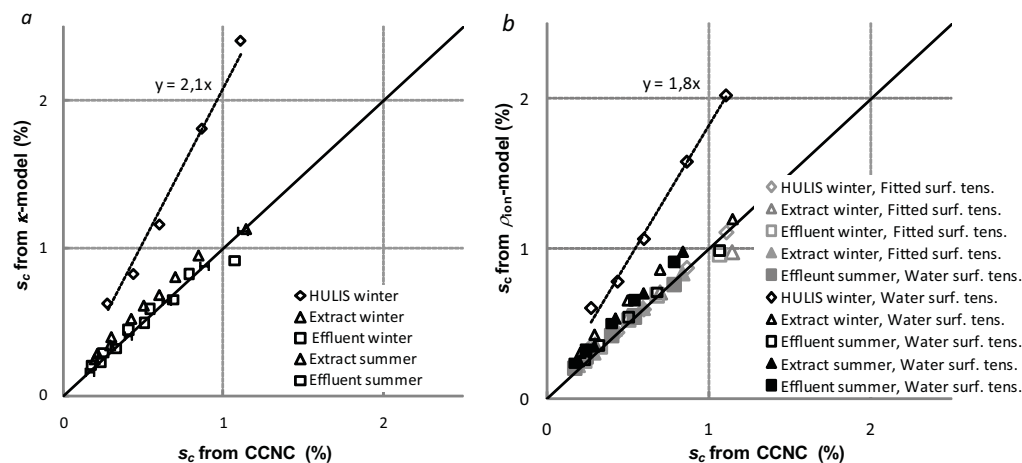


Fig. 7. Comparison of κ_R model (a) and ρ_{ion} model (b) to CCNC data for the K-pusztawinter sample. In (b) the ρ_{ion} model is shown both assuming water surface tension and fitting the surface tension to the data. In (a), the error bars along the 1:1 line represent typical uncertainties of the experimental s_c from the CCN counter.

Title Page

Abstract

Introduction

Conclusions

References

Tables

Figures

◀

▶

◀

▶

Back

Close

Full Screen / Esc

Printer-friendly Version

Interactive Discussion

Hygroscopic properties of Amazonian biomass burning

E. O. Fors et al.

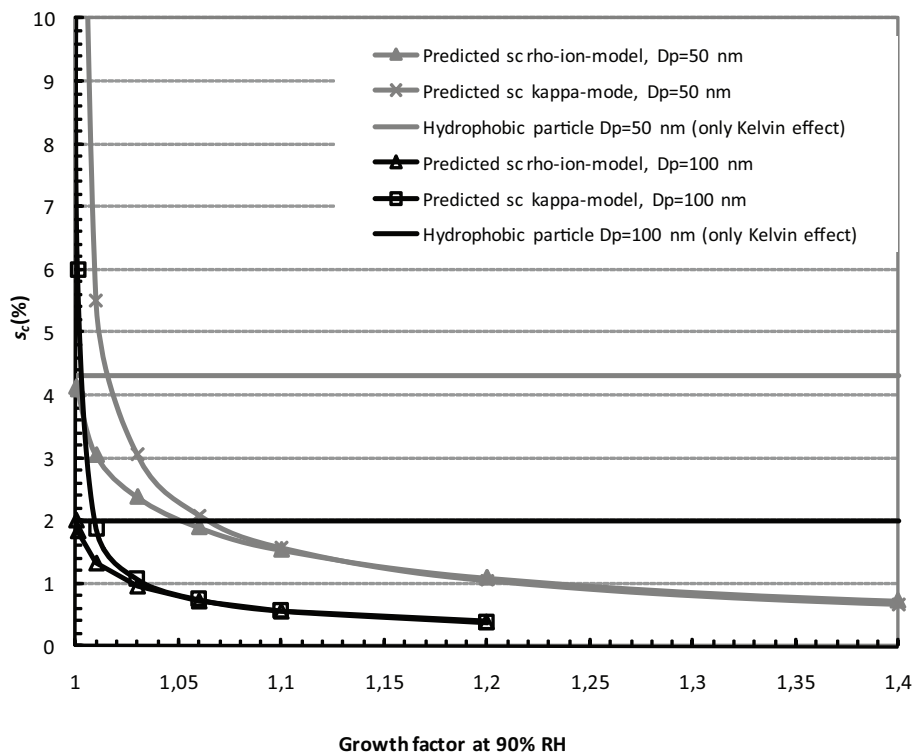


Fig. 8. Illustrating the effect on predicted supersaturation at low growth factors at 90% using the approximated Köhler theory at activation. The approximation leads to an overestimation of the critical supersaturation. The difference is getting smaller as the dry particle size or Gf increases.

[Title Page](#)[Abstract](#)[Introduction](#)[Conclusions](#)[References](#)[Tables](#)[Figures](#)[◀](#)[▶](#)[◀](#)[▶](#)[Back](#)[Close](#)[Full Screen / Esc](#)[Printer-friendly Version](#)[Interactive Discussion](#)

Hygroscopic properties of
Amazonian biomass
burning

E. O. Fors et al.

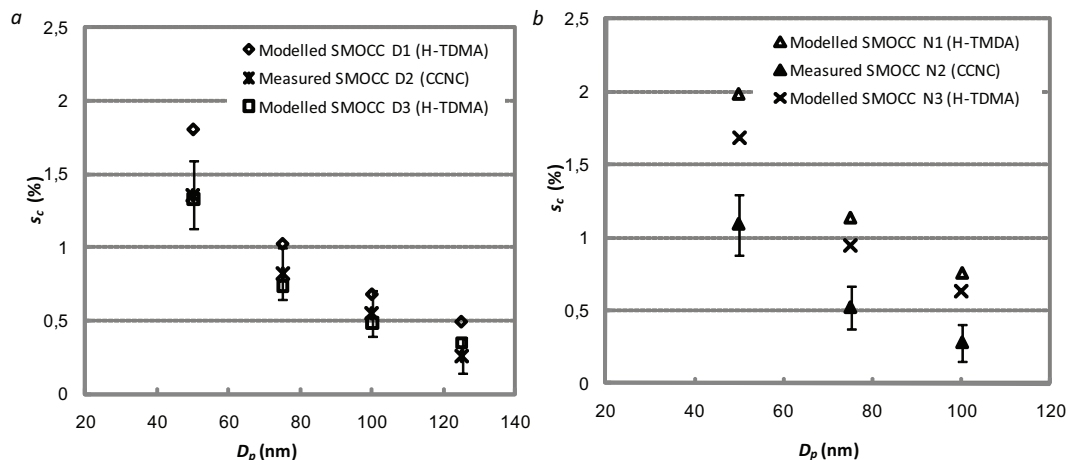


Fig. 9. Measured and modelled s_c values for the SMOCC day and night samples based on the ρ_{ion} model with water surface tension, using H-TDMA data as input. Due to the small amount of material in the sample they were analysed either by the CCNC or the H-TDMA. Therefore, the predicted s_c values are based on data before and after the CCNC period.

[Title Page](#)[Abstract](#)[Introduction](#)[Conclusions](#)[References](#)[Tables](#)[Figures](#)[◀](#)[▶](#)[◀](#)[▶](#)[Back](#)[Close](#)[Full Screen / Esc](#)[Printer-friendly Version](#)[Interactive Discussion](#)